PAPER • OPEN ACCESS

Immunomodulation of surface biofunctionalized 3D printed porous titanium implants

IOP ebooks™

Bringing together innovative digital publishing with leading authors from the global scientific community.

Start exploring the collection−download the first chapter of every title for free.

Biomedical Materials

PAPER

Immunomodulation of surface biofunctionalized 3D printed porous titanium implants

F Razzi[1,2,4], L E Fratila-Apachitei[1,4] , N Fahy[2,3], Y M Bastiaansen-Jenniskens[3], I Apachitei[1], E Farrell[2,5] and A A Zadpoor[1,5]

1 Department of Biomechanical Engineering, Faculty of Mechanical, Maritime, and Materials Engineering, Delft University of Technology (TU Delft), Mekelweg 2, 2628 CD, Delft, The Netherlands
2 Department of Oral and Maxillofacial Surgery, Erasmus MC, University Medical Center Rotterdam, Dr Molewaterplein 40, 3015 GD, Rotterdam, The Netherlands
3 Department of Orthopaedics, Erasmus MC, University Medical Center Rotterdam, Dr Molewaterplein 40, 3015 GD, Rotterdam, The Netherlands
4 First co-authors.
5 Last co-authors.

E-mail: e.l.fratila-apachitei@tudelft.nl

Abstract

Additive manufacturing (AM) techniques have provided many opportunities for the rational design of porous metallic biomaterials with complex and precisely controlled topologies that give rise to unprecedented combinations of mechanical, physical, and biological properties. These favorable properties can be enhanced by surface biofunctionalization to enable full tissue regeneration and minimize the risk of implant-associated infections (IAIs). There is, however, an increasing need to investigate the immune responses triggered by surface biofunctionalized AM porous metals. Here, we studied the immunomodulatory effects of AM porous titanium (Ti-6Al-4V) printed using selective laser melting, and of two additional groups consisting of AM implants surface biofunctionalized using plasma electrolytic oxidation (PEO) with/without silver nanoparticles. The responses of human primary macrophages and human mesenchymal stromal cells (hMSCs) were studied in terms of cell viability, cell morphology and biomarkers of macrophage polarization. Non-treated AM porous titanium triggered a strong pro-inflammatory response in macrophages, albeit combined with signs of anti-inflammatory effects. The PEO treatment of AM porous titanium implants showed a higher potential to induce polarization towards a pro-repair macrophage phenotype. We detected no cytotoxicity against hMSCs in any of the groups. However, the incorporation of silver nanoparticles resulted in strong cytotoxicity against attached macrophages. The results of this study indicate the potential immunomodulatory effects of the AM porous titanium enhanced with PEO treatment, and point towards caution and further research when using silver nanoparticles for preventing IAIs.

1. Introduction

Recent progress in additive manufacturing (AM = 3D printing) of metallic biomaterials [1–3] has enabled fabrication of volume-porous orthopedic implants with favorable properties that originate from the small-scale topological design of the underlying lattice structure. Examples are bone-mimicking mechanical [4–7] and mass transport [8–11] properties that facilitate bone tissue regeneration as well as their

highly porous structure that allows for bony ingrowth. Ideally, all or most of the pore space should be filled with *de novo* bone. In the case of temporary bone substitutes made from biodegradable metals such as magnesium [12] and iron [13], this could potentially lead to full regeneration of large bony defects and complete resorption of the implant. Animal experiments have, however, demonstrated that full regeneration of large bony defects often requires the application of biofunctionalization techniques that

enhance the bone tissue regeneration performance of AM porous metals [14, 15]. With proper biofunctionalization, full bone regeneration is possible even in critical size segmental bone defects [16].

The actual surgeries are, however, more complex, with a significant risk of implant-associated infections (IAIs) particularly for complex bony reconstructions in revision surgeries [17, 18] and treatment of bone tumors [19, 20]. This calls for an additional aim in the biofunctionalizing treatments that are applied to AM porous metals to minimize their risk of IAIs. Several studies [21–23] have shown that antibacterial surface coatings applied to such materials could both kill planktonic bacteria and prevent the formation of biofilms even in the case of multi-drug resistant strains such as methicillin-resistant *Staphylococcus aureus* [24]. The topological design of the AM porous structure could play an important role in this regard, by increasing the available surface area by several orders of magnitude and, thus, amplifying the beneficial effects of surface treatments. Indeed, a direct comparison between AM porous titanium and corresponding solid implants has shown that for the same type of antibacterial surface treatment, the zone of inhibition is several times larger in AM porous titanium as compared to the solid counterparts [24].

To address both challenges of limited bone regeneration and IAIs, it is often assumed that biofunctionalizing treatments should afford AM porous metals dual functionalities. This assumption ignores the important roles of the immune system both in regulating the bone tissue regeneration and clearing infections as well as the interplay between infection clearance and bone tissue regeneration processes [25]. It is therefore important to assess the immunomodulatory aspects of the biofunctionalizing (surface) treatments applied to AM porous metals.

The inflammatory events triggered by biomaterials have been generally perceived as being detrimental for the acceptance of the biomaterial in the host, and therefore the focus has been on minimizing inflammation. During such inflammatory responses macrophages may derive from peripheral blood monocytes and become activated, which results in a range of phenotypes encompassing pro-inflammatory (M1-like), or anti-inflammatory and tissue repair (M2-like) macrophages. More recent research shows that biomaterials can induce differential immune responses [26–28] and these may have stimulatory effects on subsequent osteogenesis [29–36]. These osteoimmunomodulatory effects involve a fine balance between the pro-inflammatory (M1-like) and pro-healing (M2-like) macrophage subsets, which are activated following implantation, and their paracrine effects on the progenitor cells. This balance can be influenced by biomaterial properties including surface chemistry, topography, and hydrophilicity.

From the research so far on titanium surfaces, it is apparent that titanium surfaces modified by anodic oxidation [37–39] induce lower pro-inflammatory response relative to the non-modified surfaces, as confirmed by enzyme-linked immunosorbent assay (ELISA) and quantitative polymerase chain reaction (qPCR) analyses of specific biomarkers in the presence or absence of lipopolysaccharide (LPS) activation. Moreover, titanium surfaces modified by plasma spraying downregulate the pro-inflammatory activity of inflammatory cells while enhancing the expression of pro-healing and osteogenic factors relative to the flat control [40]. Another titanium surface treatment frequently used for dental implants consisting of sand blasting followed by acid etching to enhance surface microroughness has been found to trigger larger pro-inflammatory responses as well as higher levels of anti-inflammatory cytokines relative to the polished titanium [41, 42]. When such surfaces were made more hydrophilic, the pro-inflammatory response was downregulated [41]. A recent mechanistic study [43] suggests that spatial confinement of macrophages reduces expression of pro-inflammatory cytokines. The effect is associated with inhibition of actin polymerization which decreases the activity of the myocardin-related transcription factor A- serum response factor (MRTF-A-SRF) complex , and consequently the inflammatory response. Although the studies on macrophage responses to various biomaterials and their underlying mechanisms are scarce relative to the studies focused on somatic and stem cells [44], their findings indicate the potential of surface-induced immunomodulation as a rational biofunctionality of implants for orchestrating the biological events leading to tissue morphogenesis.

Here, we studied, for the first time, the *in vitro* immune response triggered by AM porous titanium implants surface modified to minimize their risk of IAIs while improving the host cell response [24]. The AM implants were biofunctionalized by plasma electrolytic oxidation (PEO) in the presence of silver nanoparticles. By this method, an oxide layer with interconnected microporosity, incorporating hydroxyapatite phases and silver nanoparticles is produced in a single-step process [24].

2. Materials and methods

2.1. AM porous titanium

Volume-porous titanium (Ti-6Al-4V) implants were rationally designed for the specific *in vitro*, *ex vivo*, and *in vivo* models used for evaluating their bone regeneration performance and antibacterial properties [24]. They were fabricated with selective laser melting (SLM) (SLM-125, Realizer, Borchem, Germany) from the medical-grade (extra low interstitial (ELI), grade 23) Ti-6Al-4V powder (AP&C, Boisbriand, Quebec, Canada) with spherical particles morphology and sizes between 10 and 45 μm. The pore size of the implants did not exceed 300 μm since this size has

been shown to be optimal for bone regeneration [45, 46], while their diameter was 0.5 mm to fit into murine femoral bones. Prior to further processing or analyses, the SLM implants were sonicated for 5 min in acetone, 96% ethanol, and finally in distilled water.

2.2. PEO
The AM porous implants were either left non-treated (i.e. SLM NT group) or were biofunctionalized using a research PEO setup equipped with a computer-interfaced AC power supply, a cooling system, stainless steel circular cathodes, and double walled electrolytic cells [47]. The process was performed under galvanostatic conditions using a bi-component electrolyte containing 24.0 g l^{-1} calcium acetate hydrate (CaAc) (Sigma-Aldrich, St. Louis, USA) and 4.2 g l^{-1} calcium glycerophosphate (CaGly) (Dr Paul Lohmann GmbH, Emmerthal, Germany). The PEO process was performed both in presence (i.e. SLM PEO+Ag group) and absence (i.e. SLM PEO group) of silver nanoparticles (AgNPs) (Sigma-Aldrich, St. Louis, USA) with a size distribution between 7 and 25 nm and with a spherical shape. When present, the silver nanoparticles were dispersed in the above-mentioned electrolyte at a concentration of 3.0 g l^{-1}. The oxidation was performed for 5 min under continuous electrolyte stirring. The main PEO conditions used for each experimental group are summarized in supplementary table S1, available online at stacks.iop.org/BMM/15/035017/mmedia. During the process, the voltage transients were recorded at a sampling rate of 1 Hz. After the oxidation process, the samples were rinsed under running tap water for 2 min.

2.3. Biomaterial characterization
The surface morphology of the specimens was observed with scanning electron microscopy (SEM; SEM JSM-IT100 JEOL, Tokyo, Japan) using an electron beam energy of 20 kV and a working distance of 10 mm. Prior to imaging, the PEO-treated SLM implants were gold sputtered. Energy dispersive x-ray spectroscopy (EDS) was used to analyze the elemental composition of the surface. The concentration of the ions released in phosphate buffered saline solution (PBS) from the implants was determined with inductively coupled plasma optical emission spectrometry (ICP-OES) using a Thermo Fisher iCAP6300 Duo instrument (Thermo Fisher Scientific, Waltham, Massachusetts, United States). The specimens from the SLM PEO+Ag group were placed in brown glass vials (*n* = 3) containing 1 ml PBS solution and were incubated in a water bath at 37 °C. The PBS solution was refreshed at 0.5, 1, 2, 4, and 7 d, and the concentrations of Ag, Ca, Ti, and Al ions were measured.

2.4. Isolation of human peripheral blood monocytes
Human peripheral blood mononuclear cells (hPBMCs) were isolated from buffy coats from different healthy male blood donors purchased via the Sanquin Blood bank with ethical approval (Sanquin blood bank, Amsterdam, The Netherlands; contract number: NVT0053.01), using Ficoll (Ficoll-Paque™ PLUS, GE Healthcare, Little Chalfont, UK) density gradient separation. The buffy coat was transferred from the blood bag into a T175 flask, and was diluted with buffer containing PBS (Gibco, Thermo Fisher Scientific, Waltham, Massachusetts, USA) with 0.1% bovine serum albumin (BSA) (Sigma-Aldrich) until the end volume was approximately 240 ml. 30 ml of diluted blood was slowly added to 50 ml tubes containing 15 ml Ficoll. The tubes were then centrifuged for 15 min at 1000× g without brake, to perform density gradient separation. The hPBMCs were isolated from the plasma/Ficoll interface. hPBMCs were then labelled with 100 μl of anti-CD14 magnetic bead solution and monocytes were isolated by CD14 + magnetic-activated cell sorting (MACS) according to the manufacturer's instructions (CD14 MicroBeads human, LS columns and MidiMACS™ Separator, all from Miltenyi Biotec, Bergisch Gladbach, Germany).

2.5. Transwell culture of human monocyte-derived macrophages and SLM implants
To investigate the potential effect of ions released from the different treated titanium surfaces, an indirect assay was performed. Therefore, the SLM NT, SLM PEO and SLM PEO+Ag implants (*n* = 6 per group) with a length of 0.5 cm were sterilized by autoclaving at 121 °C for 2 h. CD14 + monocytes were seeded in a 24-well plate at a cell density of 5 × 10^5 cells/cm^2 in 1 ml X-vivo medium (Lonza, Verviers, Belgium) supplemented with 20% heat-inactivated fetal bovine serum (FBS; Lonza), 50 μg ml^{-1} gentamycin (Gibco) and 1.5 μg ml^{-1} fungizone (Gibco) [48, 49]. For each well, two implants of 0.5 cm in length were placed in the transwell insert of 5 μm pore size. Apart from the three different experimental groups, a positive control group was included in the experiment consisting of monocytes cultured without the presence of implants in the transwell. After 24 h, the medium was refreshed and after additional 72 h, the cell supernatant from each experimental group was collected to investigate the released cytokine concentrations by using ELISA; see section 2.6.4. for details. In addition, the cells were imaged by using light microscopy. The experiment was repeated for three different healthy male blood donors.

2.6. Culture of human monocyte-derived macrophages on SLM Ti-6Al-4V implants
Implants from the SLM NT, SLM PEO, and SLM PEO +Ag groups with a length of 1.0 cm were sterilized by autoclaving at 121 °C for 2 h. Each implant was placed

in a 0.2 thin wall PCR reaction tube (BIOplastics, Landgraaf, The Netherlands) with 5×10^5 CD14 + monocytes in 100 μl of X-vivo medium supplemented with 20% FBS, 50 μg ml^{-1} gentamycin and 1.5 μg ml^{-1} fungizone. The samples were incubated at 37 °C and 5% CO$_2$, and turned 180° every 30 min four times in order to enable homogeneous cell adhesion on implant surfaces. After 2 h, implants were transferred to a 48-well plate in 400 μl of X-vivo medium using sterilized tweezers. A negative control was included in the experiment, consisting of implants in X-vivo medium without cells. After 24 h of culture, the implants were transferred to a clean 48-well plate and the medium was refreshed. Three days (72 h) after refreshing, the medium was collected and the samples were prepared for investigation of cell morphology, gene expression, cytokines release, and viability.

2.6.1. Cell morphology
The morphology of monocyte-derived macrophages which attached to the implants was assessed by SEM imaging after 4 d of culture for five different donors. Therefore, the samples were firstly washed with PBS and then fixed for at least 2 h at 4 °C in a solution of PBS with 4% paraformaldehyde (PFA) and 1% glutaraldehyde. Sample dehydration was performed at room temperature using a series of increasing ethanol concentrations (i.e. 50%, 70%, and 96%). Finally, the specimens were allowed to dry overnight in a petri-dish. Prior to SEM imaging, the samples were gold sputtered for 2 min. For each surface, both secondary electron and backscattered modes were used to image the attached macrophages at different magnifications (i.e. 100×, 200×, 500×, 1000× and 2000×).

2.6.2. Cell viability
Live/dead staining (CyQuant kit) was performed to assess the viability of the adhered cells on the implants after 4 d of culture. The implants with adherent macrophages in 48-well plate were washed three times in 0.9% NaCl solution and stained with 300 μl of NaCl solution containing 0.1% of Calcein AM and 0.15% of ethidium homodimer (EthD-1). The samples were incubated at 37 °C for 40 min and rinsed three times in NaCl solution. The images were taken with a fluorescent microscope at 495/515 nm for Calcein AM and 495/635 nm for EthD-1 using a Zeiss LSM510 Meta (Carl Zeiss Microscopy, Jena, Germany).

2.6.3. Gene expression analysis
In order to assess the phenotype of monocyte-derived macrophages attached to the surface of the implants, expression of genes encoding for pro-inflammatory cytokines IL-6, TNF-α, and IL-1β (specific for an M1-like phenotype) and genes encoding for the anti-inflammatory factors IL-1RA, IL-10, and CCL18 (specific for an M2-like phenotype) was analysed. In addition, expression of genes encoding for M2-like

anti-inflammatory and tissue repair macrophage cell surface markers (CD163 and CD206, respectively) and for factors related to the tissue repair phase (VEGF and TGF-β1) were investigated (table S2). The expression of these genes was assessed by qPCR. Therefore, after 4 d of culture, the specimens with the attached macrophages were placed in a 1.5 ml tube containing 400 μl of TRIzol reagent (Thermo Fisher Scientific, Waltham, USA) and stored at −80 °C until the day of analysis. For the RNA isolation, 80 μl of chloroform was added to the specimens followed by centrifugation for 20 min at 12 000 × g and 4 °C to allow for the separation of the sample phases. RNA was isolated from the aqueous phase and 200 μl of isopropanol was added to allow for RNA precipitation. The samples were centrifuged 10 min at 12 000 × g. Precipitated RNA was washed twice with 400 μl of 75% ethanol and quantified using a NanoDrop spectrophotometer (Thermo Fischer Scientific) at 260/280 nm. After RNA quantification, cDNA was synthesized using the RevertAid First Strand cDNA Synthesis Kit (Thermo Fischer Scientific). Therefore, 110 ng of RNA was incubated with 0.5 μl of Oligo-d(T)18 primer, 0.5 μl Random Hexamer primer and distilled H$_2$O for 5 min at 70 °C. After incubation, the tubes were cooled on ice for 5 min and the enzyme mix containing reaction buffer, dNTPs, Ribolock inhibitor, and RevertAid M-MulV Reverse Transcriptase was added. A control without Reverse Transcriptase and one containing only distilled H$_2$O were also included. Next, the tubes were incubated for 5 min at 25 °C, 60 min at 42 °C and 10 min at 70 °C. After cooling to 12 °C, 100 μl distilled H$_2$O was added to dilute the cDNA of each sample. qPCR analysis was then performed to quantify gene expression. For each gene, a mastermix was prepared, consisting of 5.0 μl of 2× qPCR mastermix (Sybr green or taqman) and 0.5 μl of primer mix. 5.5 μl of mastermix and 4.5 μl of cDNA were added to a pre-cooled PCR plate and gene expression was quantified using a Bio-Rad CFX96 Real-Time PCR Detection system (Bio-Rad, Hercules, CA, USA). Glyceraldehyde-3-phosphate dehydrogenase (GAPDH) and hypoxanthine phosphoribosyl transferase 1 (HPRT1) were tested as housekeeper genes. The gene expression relative to GAPDH expression was determined by the $2- \Delta Ct$ formula, where $\Delta Ct = Ct_{sample} - Ct_{GAPDH}$. Gene expression analysis was performed for five different donors. All the primers used for the qPCR analysis are listed in table S3.

2.6.4. Protein quantification
In order to evaluate the concentration of pro-inflammatory cytokines (i.e. IL-6 and TNF-α) and tissue repair-related chemokines (i.e. CCL18) released in the cell supernatant, commercially available ELISA kits were used (DuoSet Development Kit; R&D Systems). After 4 d of culture, cell supernatants were centrifuged for 5 min at 500 × g, aliquoted in 200 μl and stored at

$-80\,^{\circ}$C until the analysis was performed according to the manufacturer's instructions. The assay was repeated for three (figure 2) or five (figure 5) different donors.

2.7. Culture of human mesenchymal stromal cells on implants

Human mesenchymal stromal cells (hMSCs) were isolated from leftover iliac crest bone chip material obtained from pediatric patients undergoing alveolar bone graft surgery [50]. Samples were harvested with the approval of the Erasmus Medical Ethical Committee (MEC-2014-16). Written consent was not required according to institutional guidelines for the use of waste surgical material, however an opt out was available. Cells were plated at approximately 2300 cells cm^{-2} in complete expansion medium (α-MEM containing 10% fetal bovine serum (lot# 41Q204K, Gibco)), 50 μg ml^{-1} gentamycin and 1.5 μg ml^{-1} fungizone supplemented with 25 μg ml^{-1} L-ascorbic acid 2-phosphate and 1 ng ml^{-1} fibroblast growth factor-2 (Instruchemie, Delfzijl, Netherlands) and incubated at 37 $^{\circ}$C and 5% CO$_2$ in a humidified atmosphere. The medium was refreshed every 3–4 d until cells reached approximately 80%–90% confluency. The implants ($n = 4$/group) with a length of 1.0 cm each were sterilized by autoclaving at 121 $^{\circ}$C for 2 h. The seeding protocol used was the same as described in section 2.6. In brief, specimens from the SLM NT, SLM PEO and SLM PEO+Ag groups were placed in 0.2 PCR thin wall reaction tubes with 1.5 × 105 hMSCs in 100 μl of α-MEM supplemented with 10% FBS, 50 μg ml^{-1} gentamycin, 1.5 μg ml^{-1} fungizone, 1 ng ml^{-1} fibroblast growth factor-2 (FGF-2) and 10^{-4} M vitamin C. The specimens were then incubated at 37 $^{\circ}$C and 5% CO$_2$, and turned 180° every 30 min four times in order to enable homogeneous cell adhesion on the implant surfaces. After 2 h, the specimens were transferred to a 48-well plate in 400 μl of culture medium using sterilized tweezers. The medium was refreshed after 24 h and cell morphology and viability were assessed after additional 72 h by using SEM imaging and live/dead staining following the protocols described for human macrophages.

2.8. Statistical analysis

IBM SPSS 24.0 was used for statistical analysis. After testing normal distribution of the values, linear mixed models followed by Bonferroni *post-hoc* correction were used to determine the statistical significance of the difference between various experimental groups. The experimental groups SLM NT, SLM PEO, and SLM PEO+Ag were considered as fixed factors and donors as random factors. The correlated *p*-values are presented in the results. The differences between the means were considered statistically significant when $p < 0.05$.

3. Results

3.1. Surface characteristics

The AM implants (SLM NT group) possessed the rationally designed 3D volume-porous structure with struts that exhibited spherical Ti-6Al-4V particles on their smooth, molten surface (figure 1(a)). Following PEO treatment, the surface morphology changed significantly through formation of an interconnected microporous structure over the entire 3D structure of the implants (figure 1(b)). The spherical particles were therefore less visible, becoming better integrated in the implant structure (figure 1(b)). In addition, the surface showed enhanced local roughness (figure 1(b)). No noticeable differences in the surface morphology were observed following PEO treatment in the presence of AgNPs, reflected also in the similar voltage transients and sparks evolution during the oxidation of both types of implants (figure 1(c)).

The PEO process led to various surface chemistries both with and without AgNPs (figures 1(d)–(f)). Ca and P elements from the electrolyte together with substrate elements (Ti, Al, V) and oxygen were identified in the EDS spectra of the SLM PEO implants (figure 1(e)). In the case of the SLM PEO+Ag group, additional Ag peaks associated with nanoparticles embedded in the oxide matrix appeared in the EDS spectra (figure 1(f)). Previous analysis by x-ray diffraction of the SLM PEO-treated implants [24] has indicated the development of crystalline titanium oxide phases, especially the rutile phase, as well as a hydroxyapatite, a calcium titanate, and other calcium phosphate phases.

3.2. Protein levels and morphology of human macrophages in indirect cultures

The SLM PEO+Ag implants released around 0.5 ppm Ag ions after 4 d of incubation in PBS (figure 2(a)). The release rates were higher after 0.5 and 1 d (figure 2(a)). Comparable profiles were obtained for Al and Ti ions (figure 2(a)). By comparison, Ca ions showed the highest concentrations reaching a cumulative value of ca 14 ppm after 4 d (figure 2(a)). Calcium is present in the PEO electrolyte as calcium acetate and calcium glycerophosphate. During the PEO process, ions from the electrolyte are incorporated in the growing oxide layer. Different Ca/P-based compounds may be formed in the layer depending on the PEO conditions [24]. During immersion in aqueous solutions, ionic species of Ca, P are released from such surfaces. The protein profile of macrophages after 4 d of culture showed no significant differences between cells cultured in indirect contact with the three different implant types (figure 2(b)). In addition, the protein levels were similar to the controls (i.e. cells cultured in the absence of implants) for all the markers measured (figure 2(b)). The cells released both pro- and anti-inflammatory proteins at various levels, namely
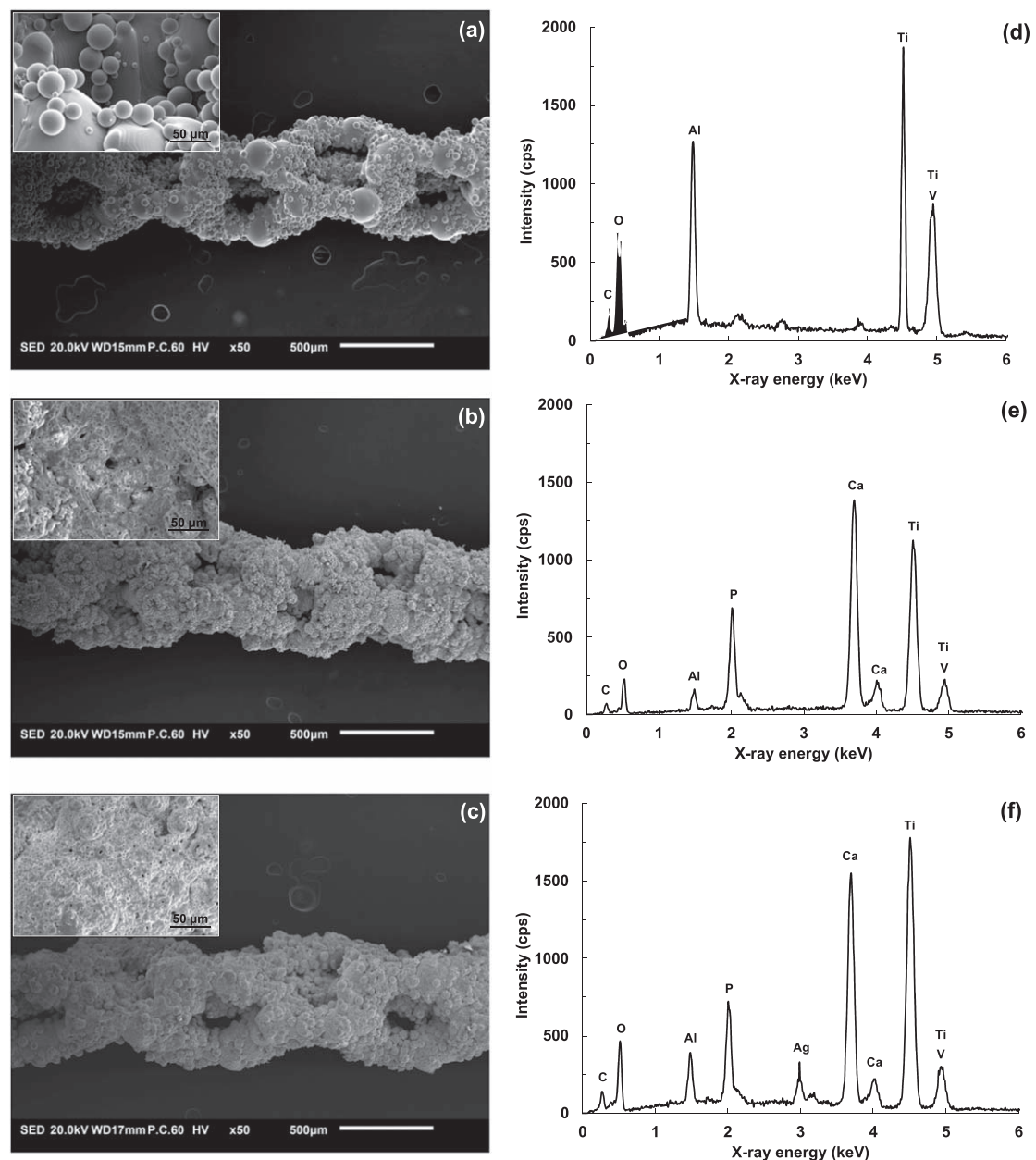
Figure 1. SEM images and EDS spectra of the SLM NT (a), (d), SLM PEO (b), (e) and SLM PEO+Ag (c), (f) implants.
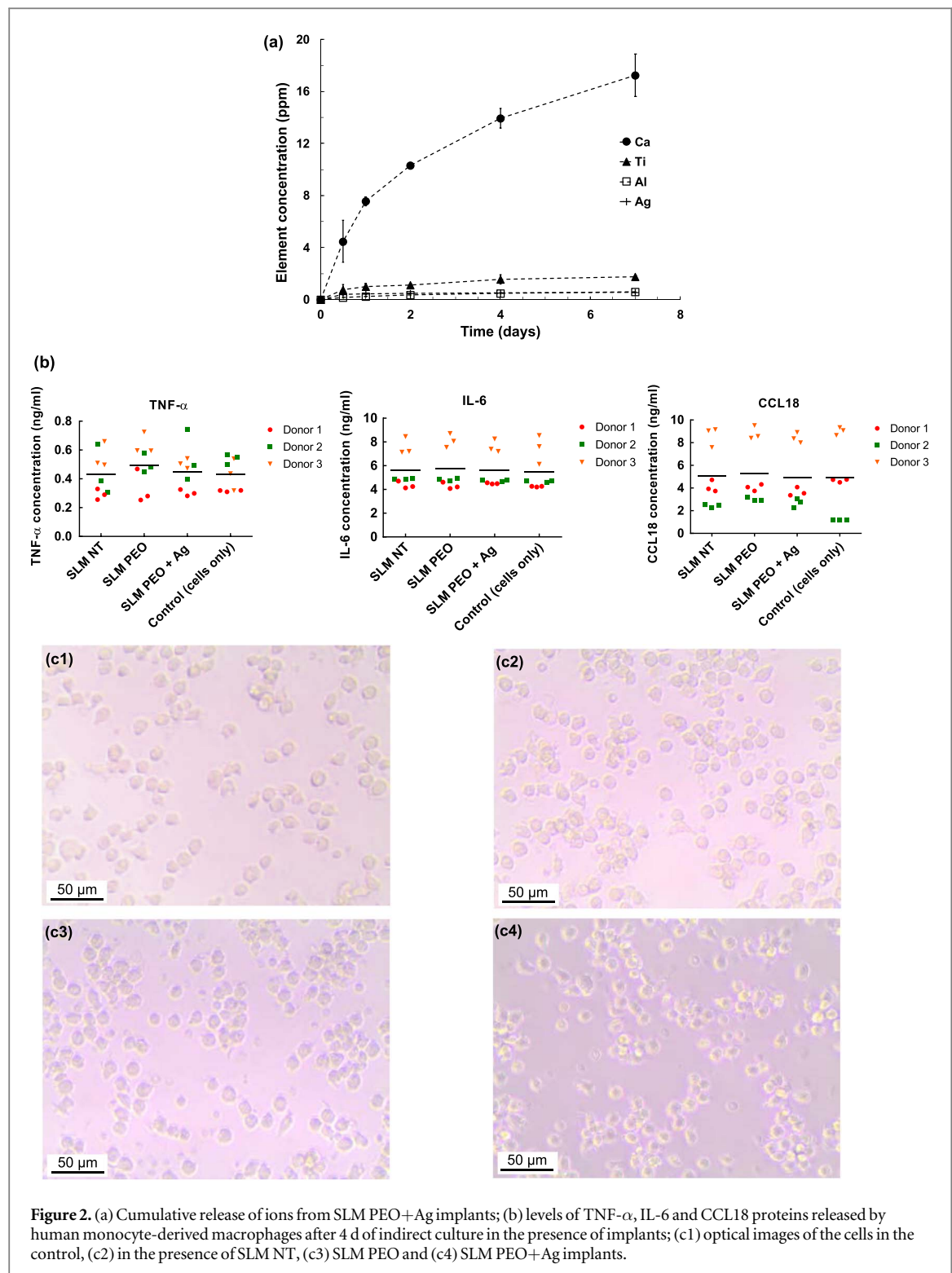
around 5 ng ml^{-1} for IL-6 and CCL18, and around 0.4 ng ml^{-1} for TNF-α (figure 2(b)). In addition, the optical imaging of the cells showed similar shapes and sizes of cells in all experimental groups (figures 2(c1)–(c4)). These findings indicate that none of the ions released by these surfaces influenced macrophage behavior.

3.3. Response of human macrophages attached to the implant surfaces

The macrophages attached uniformly to all SLM implants, as indicated by SEM images captured in the backscattered mode at various magnifications (figures 3(a)–(f)). On the SLM NT implants, the cells revealed mostly a round shape of ca. 5–10 μm in size and very fine cellular extensions helping their

attachment on the locally smooth surface (figures 3(a), (b)). Cell–cell contacts were also visible after 4 d of culture (figures 3(a), (b)). On the SLM PEO implants, cells showed a relatively spread morphology and more cell–cell contacts (figures 3(c), (d)). By comparison, macrophages attached to the surface of the SLM PEO +Ag implants spread less and showed a predominantly round and flat morphology (figures 3(e), (f)). No variability in cell morphology was observed between the different donors investigated.

From the ten different genes analyzed by qPCR (table S3), nine were detected on SLM NT, seven on SLM PEO and none on the SLM PEO+Ag specimens (figure 4). This trend was consistent for the five different donors tested (figure 4). All the three pro-inflammatory genes (IL-1*b*, TNF-*a*, IL-6*)* were expressed on

Figure 2. (a) Cumulative release of ions from SLM PEO+Ag implants; (b) levels of TNF-α, IL-6 and CCL18 proteins released by human monocyte-derived macrophages after 4 d of indirect culture in the presence of implants; (c1) optical images of the cells in the control, (c2) in the presence of SLM NT, (c3) SLM PEO and (c4) SLM PEO+Ag implants.

the SLM NT implants (figures 4(a)–(c)). By comparison, on the SLM PEO surfaces, only the TNF-*a* could be detected and the levels were significantly lower ($p < 0.05$) than on the SLM NT implants (figure 4(a)). In the case of the anti-inflammatory genes, six out of seven genes were detected on both implants, albeit at different levels (figures 4(d)–(i)). Significantly higher expression of IL-1RA ($p < 0.0001$) and CD206 ($p < 0.01$) was detected on the SLM NT specimens (figures 4(d), (h)) whereas CD163 was significantly

more expressed on the SLM PEO surfaces ($p < 0.01$) (figure 4(g)). The gene expression levels of CCL18, IL-10, and TGF-*b*1 were comparable on SLM NT and SLM PEO specimens whereas VEGF was not detected on any specimens (figures 4(e), (f), (i)).

In a similar manner to gene expression levels, ELISA measurements showed that PEO treatment induced significantly lower protein levels of the pro-inflammatory cytokine IL-6 ($p < 0.0001$) and similar levels of the wound-healing related chemokine CCL18
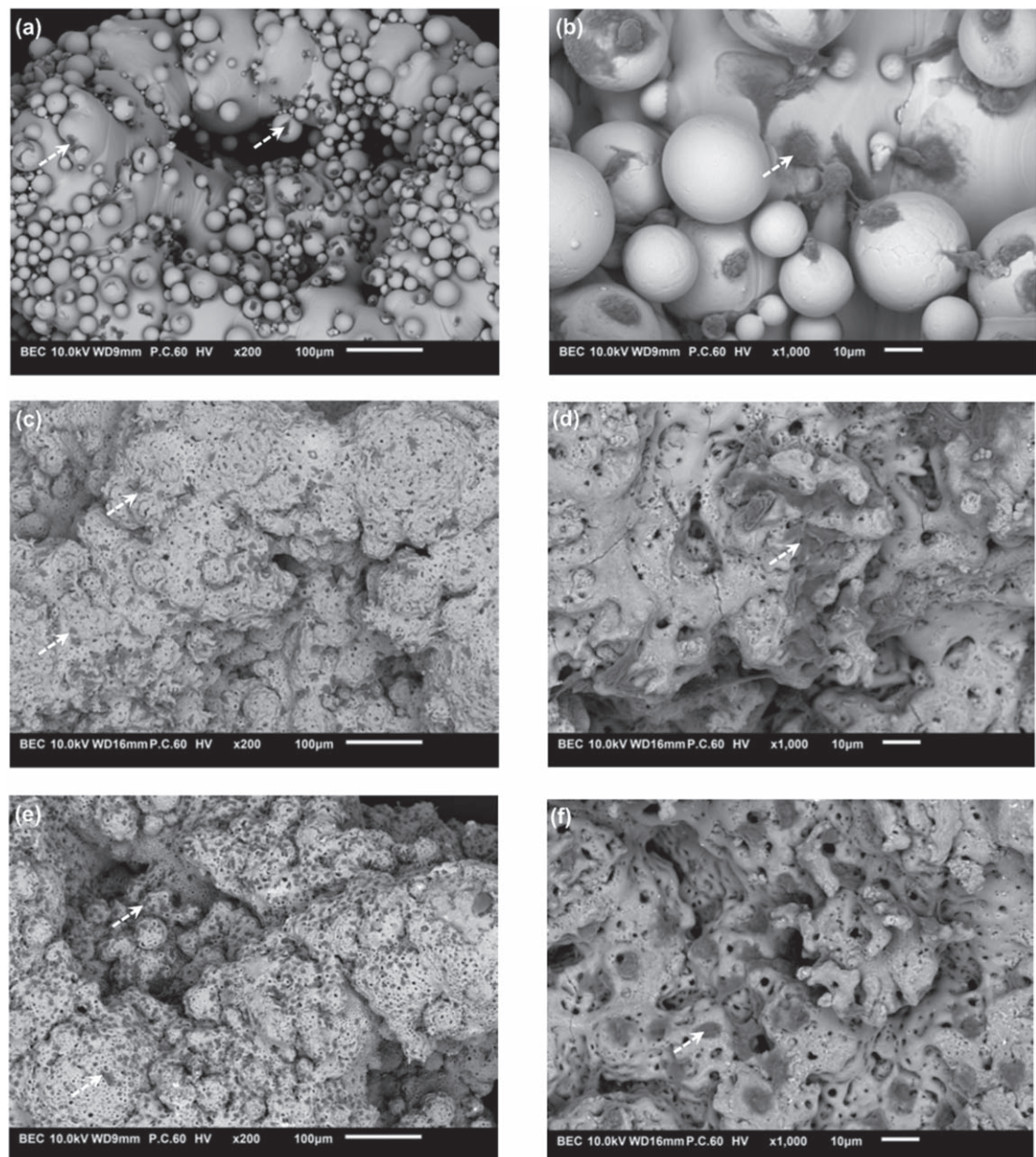
Figure 3. SEM images of the human monocyte-derived macrophages (indicated by the white arrows) attached on: (a), (b) SLM implants; (c), (d) SLM PEO implants; (e), (f) SLM PEO+Ag implants after 4 d of culture.

compared to the non-treated surfaces (figure 5). As in the case of gene expression analysis, none of the proteins investigated were detected on the SLM PEO+Ag specimens (figure 5).
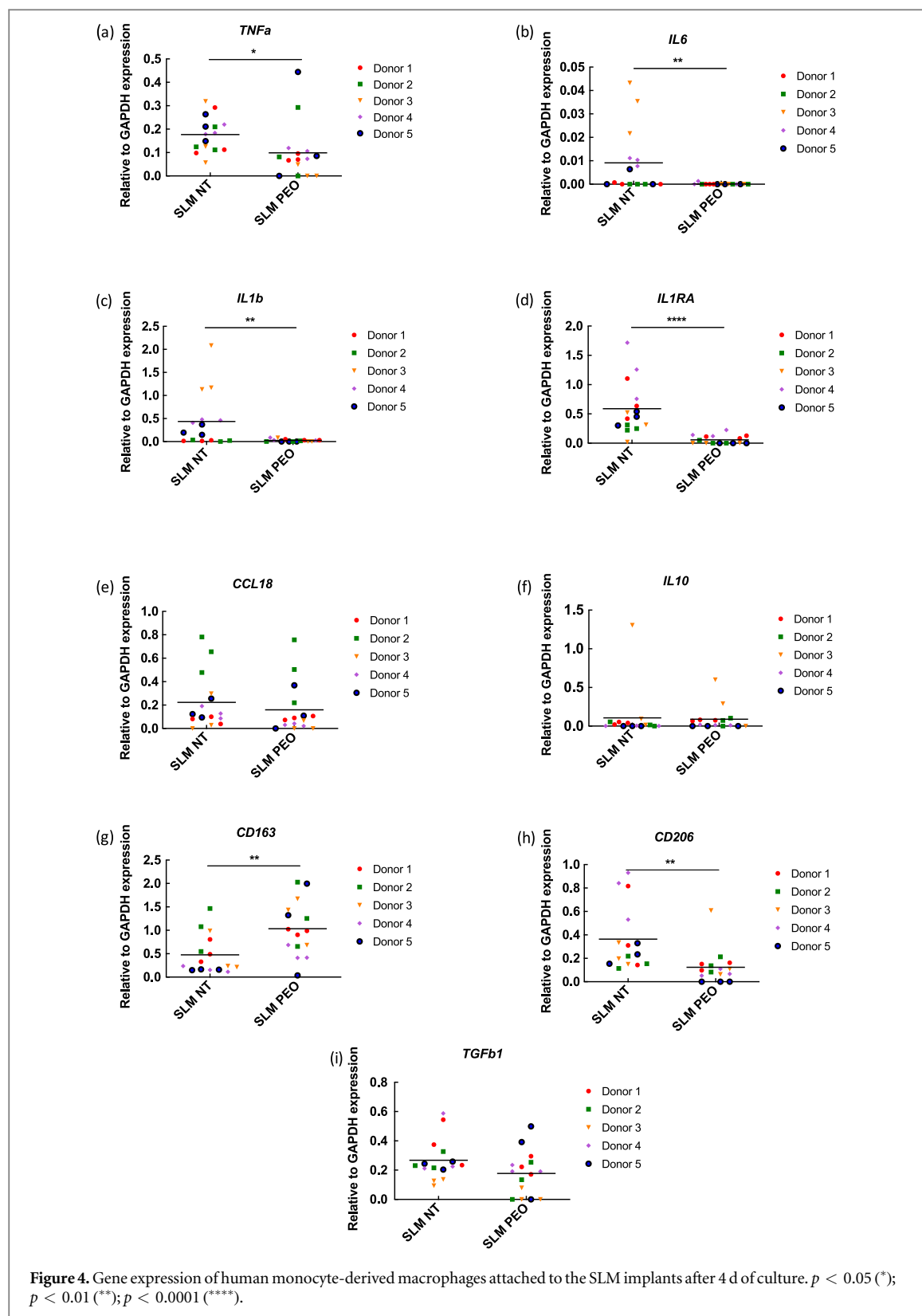
Taken together, the findings on gene and protein expression indicate that the SLM PEO implants have potential immunomodulatory effects as evidenced by a reduced pro-inflammatory response (both at the gene and protein levels) relative to the SLM NT implants and a higher potential to enhance polarization towards M2-like macrophage phenotype.

The viability of the inflammatory cells attached to the three different types of implants, as indicated by live/dead staining, revealed, as expected, that the cells could survive on the SLM NT and SLM PEO surfaces (figures 6(a), (b)). However, the SLM PEO+Ag

implants proved to be cytotoxic for these cells, explaining the results of the gene and protein analyses obtained for this type of implant (figure 6(c)).

3.4. Viability and morphology of hMSCs

hMSCs survived on all surfaces (figure 7) indicating that the SLM PEO+Ag implants were not cytotoxic for these cells, a finding supported by our previous research [24] and indicating possible different levels of Ag toxicity for these two different types of cells. In addition, hMSCs attached uniformly on all specimens and covered almost the entire surface of the 3D porous structures after 4 d of culture (figure 8). They showed a full spread morphology and larger sizes relative to human macrophages being able to bridge the pores of the SLM implants (figures 8(a), (c), (e)). These results

Figure 4. Gene expression of human monocyte-derived macrophages attached to the SLM implants after 4 d of culture. $p < 0.05$ (*); $p < 0.01$ (**); $p < 0.0001$ (****).

suggest that all the specimens from all groups supported the early cellular functions of these cells.

4. Discussion

The present study investigated for the first time the response of human primary macrophages to AM porous titanium implants produced by SLM and further modified by PEO under two different conditions. Whereas macrophage behavior was not affected by the ions released from the implants, a differential response was generated upon direct contact with the implant surfaces.

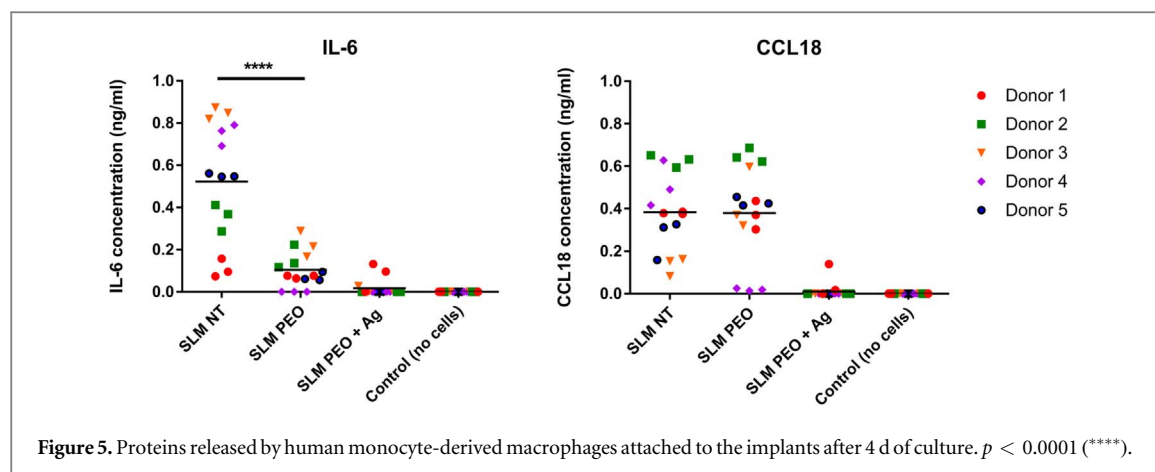The SLM NT implants elicited the strongest inflammatory response characterized by relatively

Figure 5. Proteins released by human monocyte-derived macrophages attached to the implants after 4 d of culture. $p < 0.0001$ (****).

high levels of IL-6, TNF-*a*, and IL-1*b* pro-inflammatory genes. IL-6 is mostly secreted by M1-like macrophages [50, 51] and may inhibit differentiation and maturation of osteoblasts [52]. Furthermore, prolonged expression of this cytokine may suggest formation of granulation tissue as part of the wound healing process [53, 54]. TNF-*a* and IL-1*b* are considered indicators of an acute pro-inflammatory response [52]. Such factors recruit other inflammatory cells to the implant site. Indeed, some studies have reported that they can induce osteoblast apoptosis as well as inhibit osteogenic differentiation, having detrimental effects on healing, both *in vitro* and *in vivo* [55–57]. TNF-*a* and IL-1*b* have also been shown to be implicated in angiogenesis and the regulation of osteoblast and fibroblast proliferation during wound healing [58, 59].

Macrophages cultured on SLM NT implants also expressed anti-inflammatory genes, with higher IL-1RA and CD206 levels as compared to the SLM PEO surfaces. IL-1RA is mostly present in the early stages of the inflammation phase with the main role of inhibiting the expression of pro-inflammatory cytokines [28, 60] whereas the presence of CD206, which is a surface marker of M2-like tissue repair macrophages, reflects the onset of the wound healing process. Furthermore, the presence of both IL-1*b* and TGF-*b*1 indicate the transition from a M1-like phenotype, associated with upregulation of IL-1*b*, to a M2-like phenotype when TGF-*b*1 plays a crucial role [61] by enhancing the proliferation and differentiation of osteoblast precursors and stimulating angiogenesis [62]. Therefore, the results indicate that after 4 d, the SLM NT implants led to an acute pro-inflammatory response and possible onset of the tissue repair phase.

Surface biofunctionalization of SLM implants by PEO changed the inflammatory response of the human primary macrophages. A significant downregulation of pro-inflammatory cytokines was observed at both gene and protein levels. From the M2-like markers, IL-1RA gene was strongly downregulated whereas CD163 was upregulated. CD163 is a surface marker of anti-inflammatory M2-like macrophages involved in the downregulation of pro-

inflammatory factors [63]. The downregulation of the pro-inflammatory factors and the absence of IL-6, together with the very low levels of IL-1RA and the presence of CCL18 and TGF-*b*1 indicate a dominant pro-repair microenvironment generated by cells cultured on the PEO-treated SLM implants. Smoothening of the SLM NT surfaces following PEO and the presence of the micropores have contributed to the change in macrophage morphology. These changes could influence their polarization behavior [29]. Nevertheless, since both surface topography and surface chemistry are changed by the PEO process, a combined effect cannot be excluded. The very few studies recently published on macrophage response to PEO surfaces [29, 64] indicate the osteoimmunomodulatory potential of such surfaces. Namely, PEO layers produced on pure titanium and post-heat treated at 650 °C showing the interconnected PEO microporosity, hydrophilic properties, and crystalline hydroxyapatite nanoparticles, suppressed the pro-inflammatory response of murine macrophages and upregulated expression of the anti-inflammatory macrophage marker CD163 [29], in line with our findings. In another study, PEO layers produced in electrolytes containing Ca, Si, and Cu-based compounds showed a favorable inflammatory response [64].

Incorporation of AgNPs on the surface of SLM PEO implants for providing antibacterial functionality led to cytotoxic effects for the human-blood derived macrophages. Although the cells attached on these surfaces, they remained round and flat, indicating inactive cells [29]. The gene and protein analyses supported the morphological findings, and the viability tests confirmed cells death after 4 d of culture on these surfaces. The fact that the same type of macrophages was not affected by the ions released from this implant suggests that the contact with the PEO surfaces bearing the AgNPs is inducing cell death. Interestingly, the same surfaces revealed no sign of toxicity for the hMSCs. Moreover, in a previous study [24] we have investigated the effects of such surfaces on the metabolic activity of hMSCs during one week of culture. The findings showed no significant difference in the
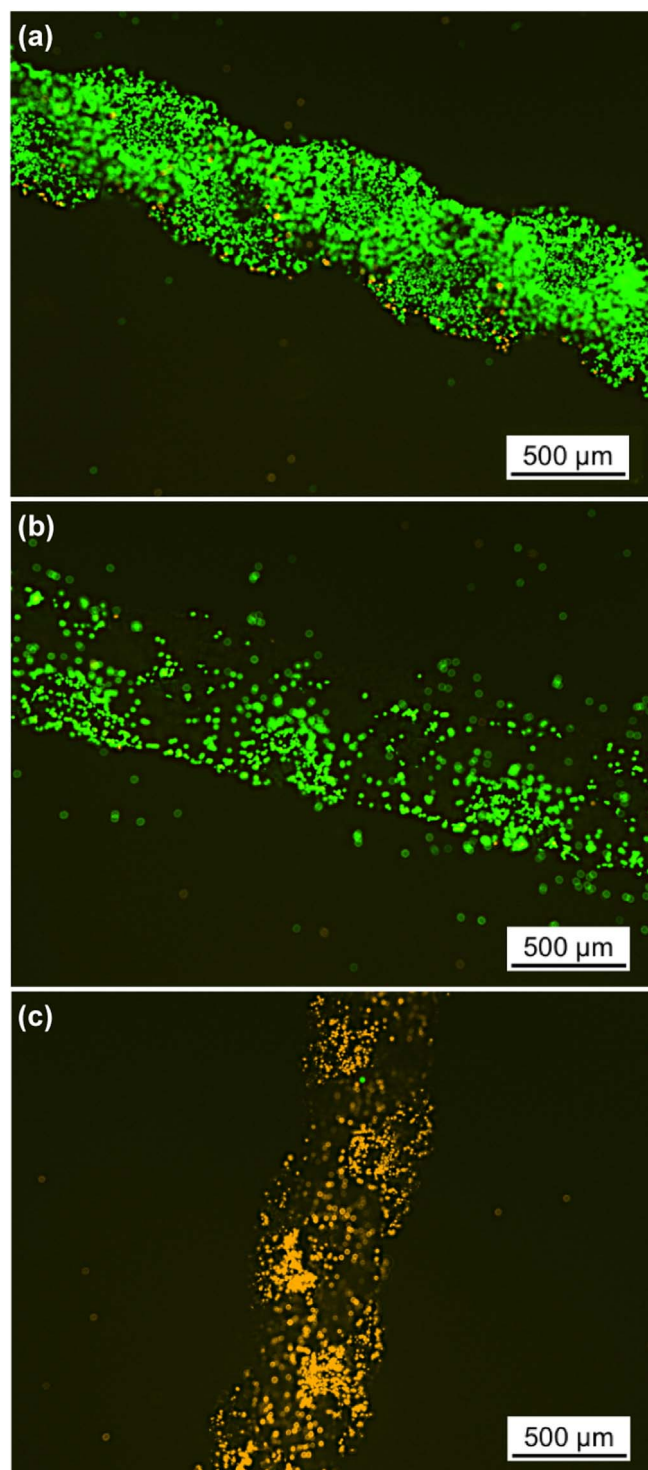
Figure 6. Live/dead staining of the human monocyte-derived macrophages attached to: (a) SLM NT; (b) SLM PEO; (c) SLM PEO +Ag implants after 4 d of culture. Green colour indicates the live cells and orange colour the dead cells.

metabolic activity of the hMSCs cultured on the three different surfaces within the first 4 d of culture. These indicate that growth and/or proliferation of these cells in the first four days of culture on the three different surfaces are/is comparable. Therefore, the human primary macrophages seem to be more sensitive to the presence of AgNPs and such surfaces may lead to a compromised immune system response *in vivo*, as recently observed with Ag bearing titanium surfaces

[23]. The results reported in this research are in line with previous *in vitro* studies, which show that macrophages, compared to other cell types, are more sensitive to the toxic effects of AgNPs [65]. Particles uptake and ROS production are higher in macrophages as compared to epithelial, hepatic, and neuronal cells. Macrophages are phagocytic cells and internalization of AgNPs through scavenger receptors present on cell membrane can occur. Once in the cells, AgNPs release
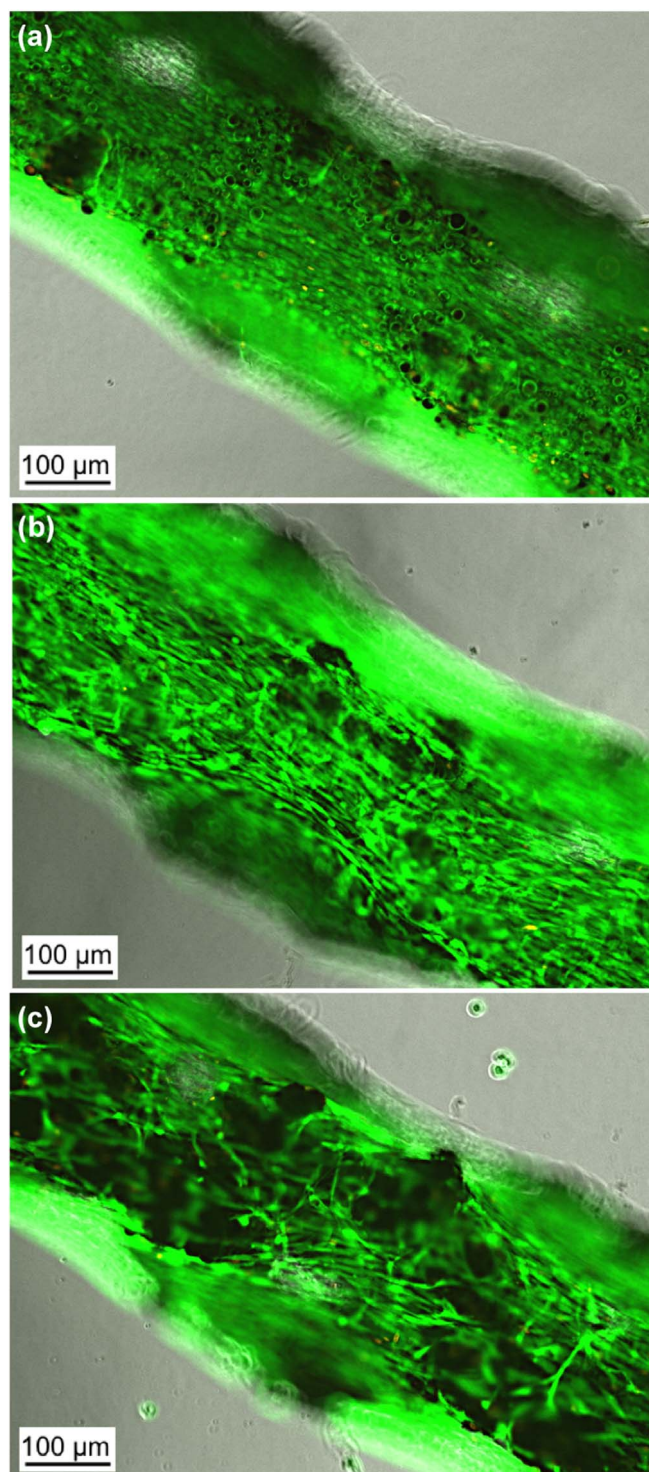
Figure 7. Live/dead staining of the hMSCs attached to: (a) SLM NT; (b) SLM PEO; (c) SLM PEO+Ag implants after 4 d of culture. Green colour indicates the live cells.

Ag ions, which may lead to oxidative stress due to free radical production. This may result in mitochondrial damage, inducing apoptotic cell death [66]. However, in the case of SLM PEO+Ag surfaces, the AgNPs cannot be taken up by the cells as they are attached to the surface of these implants. Therefore, other possible mechanisms or triggers should be considered. Attempted phagocytosis may be one of them. The consequent damaging effects of the cell membrane associated with possible high local concentrations of Ag ions and induced ROS formation could activate signaling pathways (inflammasome activation) that can eventually lead to cell death [67, 68]. More studies are required to investigate these possible mechanisms and
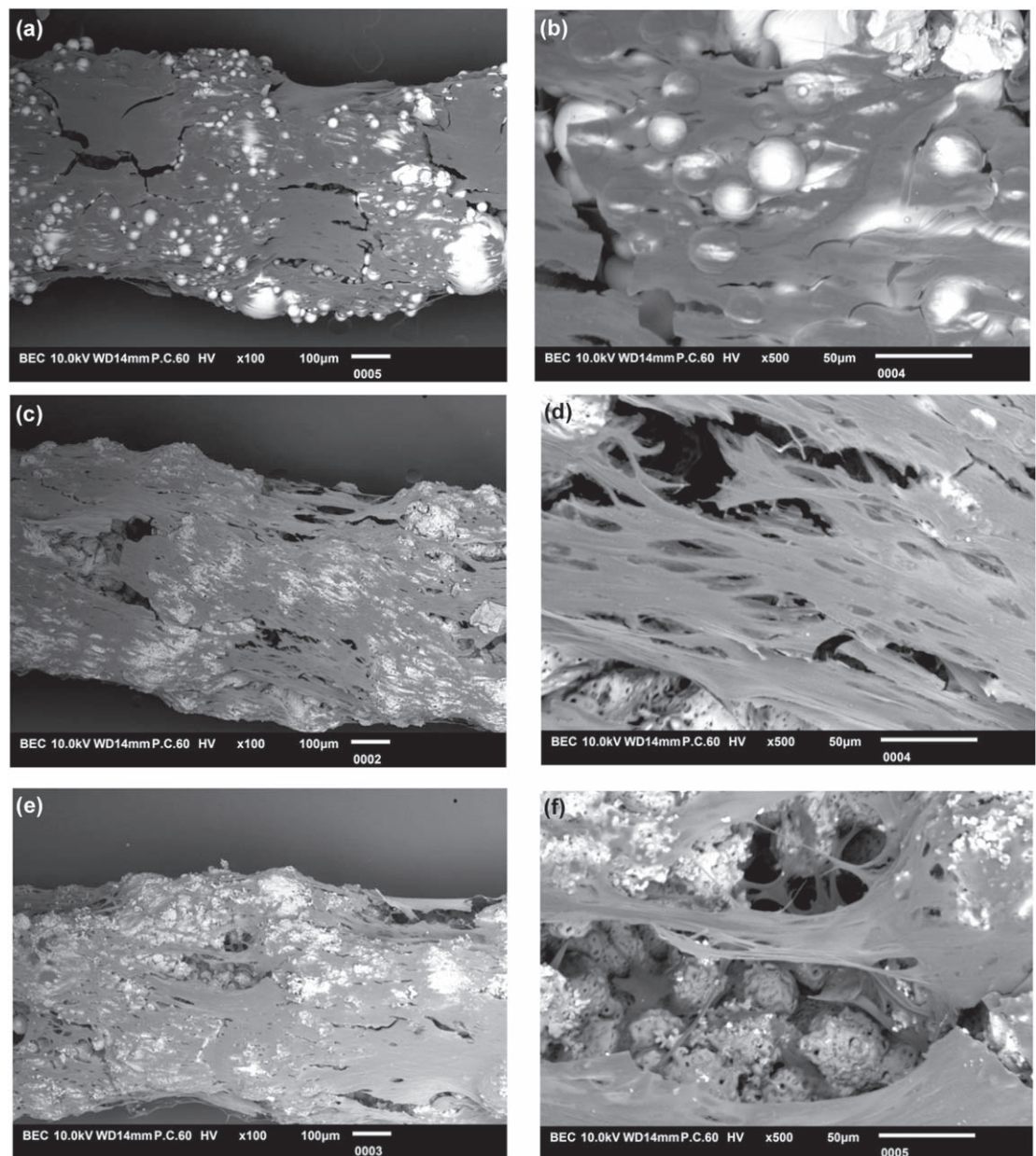
Figure 8. SEM images of the hMSCs attached to: (a), (b) SLM NT; (c), (d) SLM PEO; (e), (f) SLM PEO+Ag implants after 4 d of culture.

to optimize the AgNPs level in the PEO layer to ensure the required sustained antibacterial function without being cytotoxic for the macrophages.

On the other hand, this study indicates the favorable immunomodulatory effects of the SLM PEO implants and their support for the early function of the hMSCs. Since the immune response is also responsible for the removal of pathogens from the surgical site, the possible early antibacterial potential of the microenvironment generated by the attached macrophages should be addressed in addition to the effects of the observed immune response on osteogenesis. In this way, the potential of the immune response for both tissue regeneration and antibacterial activity can be revealed and used in the endeavor of creating safe and increasingly functional AM titanium bone implants.

5. Conclusions

In summary, this study reveals for the first time the response of human primary macrophages to AM titanium implants having three different surface conditions, namely as built, PEO-treated, and PEO-treated in the presence of AgNPs. Significantly different responses were obtained ranging from cytotoxic effects in the case of AgNPs-bearing surfaces to strong pro-inflammatory effects combined with an early anti-inflammatory response in the case of as built AM implants, and a dominant pro-repair response in the case of PEO-treated implants. The immunomodulatory effects observed for the combination of the AM and PEO surface modification should be further explored and harnessed for the

interrelated osteoimmunomodulation and antibacterial functionalities.

ORCID iDs

L E Fratila-Apachitei ⬤ https://orcid.org/0000-0002-7341-4445

References

[1] Li S *et al* 2014 Influence of cell shape on mechanical properties of Ti–6Al–4V meshes fabricated by electron beam melting method *Acta Biomater.* **10** 4537–47

[2] Van Hooreweder B, Apers Y, Lietaert K and Kruth J-P 2017 Improving the fatigue performance of porous metallic biomaterials produced by selective laser melting *Acta Biomater.* **47** 193–202

[3] Wauthle R *et al* 2015 Revival of pure titanium for dynamically loaded porous implants using additive manufacturing *Mater. Sci. Eng.* C **54** 94–100

[4] Ahmadi S *et al* 2018 Fatigue performance of additively manufactured meta-biomaterials: the effects of topology and material type *Acta Biomater.* **65** 292–304

[5] Hedayati R *et al* 2018 Isolated and modulated effects of topology and material type on the mechanical properties of additively manufactured porous biomaterials *J. Mech. Behav. Biomed. Mater.* **79** 254–63

[6] Hedayati R, Sadighi M, Mohammadi-Aghdam M and Zadpoor A 2016 Mechanical properties of regular porous biomaterials made from truncated cube repeating unit cells: analytical solutions and computational models *Mater. Sci. Eng.* C **60** 163–83

[7] Zadpoor A A 2017 Mechanics of additively manufactured biomaterials *J. Mech. Behav. Biomed. Mater.* **70** 1–6

[8] Bobbert F *et al* 2017 Additively manufactured metallic porous biomaterials based on minimal surfaces: a unique combination of topological, mechanical, and mass transport properties *Acta Biomater.* **53** 572–84

[9] Montazerian H, Davoodi E, Asadi-Eydivand M, Kadkhodapour J and Solati-Hashjin M 2017 Porous scaffold internal architecture design based on minimal surfaces: a compromise between permeability and elastic properties *Mater. Des.* **126** 98–114

[10] Truscello S, Kerckhofs G, Van Bael S, Pyka G, Schrooten J and Van Oosterwyck H 2012 Prediction of permeability of regular scaffolds for skeletal tissue engineering: a combined computational and experimental study *Acta Biomater.* **8** 1648–58

[11] Zhang X-Y, Fang G, Leeflang S, Zadpoor A A and Zhou J 2019 Topological design, permeability and mechanical behavior of additively manufactured functionally graded porous metallic biomaterials *Acta Biomater.* **84** 437–52

[12] Li Y *et al* 2018 Additively manufactured biodegradable porous magnesium *Acta Biomater.* **67** 378–92

[13] Li Y *et al* 2018 Additively manufactured biodegradable porous iron *Acta Biomater.* **77** 380-393

[14] Van der Stok J *et al* 2013 Selective laser melting-produced porous titanium scaffolds regenerate bone in critical size cortical bone defects *J. Orthopaedic Res.* **31** 792–9

[15] Yavari S A *et al* 2014 Bone regeneration performance of surface-treated porous titanium *Biomaterials* **35** 6172–81

[16] Van der Stok J *et al* 2015 Full regeneration of segmental bone defects using porous titanium implants loaded with BMP-2 containing fibrin gels *Eur. Cells Mater.* **2015** 141–54

[17] Kunutsor S K, Whitehouse M R, Lenguerrand E, Blom A W, Beswick A D and Team I 2016 Re-infection outcomes following one-and two-stage surgical revision of infected knee prosthesis: a systematic review and meta-analysis *PLoS One* **11** e0151537

[18] Mortazavi S J, Schwartzenberger J, Austin M S, Purtill J J and Parvizi J 2010 Revision total knee arthroplasty infection: incidence and predictors *Clin. Orthopaedics Relat. Res.*® **468** 2052–9

[19] Jeys L, Grimer R, Carter S and Tillman R 2005 Periprosthetic infection in patients treated for an orthopaedic oncological condition *J. Bone Joint Surg. Am.* **87** 842–9

[20] Pala E, Trovarelli G, Calabrò T, Angelini A, Abati C N and Ruggieri P 2015 Survival of modern knee tumor megaprostheses: failures, functional results, and a comparative statistical analysis *Clin. Orthopaedics Relat. Res.* **473** 891–9

[21] Amin Yavari S *et al* 2016 Antibacterial behavior of additively manufactured porous titanium with nanotubular surfaces releasing silver ions *ACS Appl. Mater. Interfaces* **8** 17080–9

[22] Bakhshandeh S *et al* 2017 Simultaneous delivery of multiple antibacterial agents from additively manufactured porous biomaterials to fully eradicate planktonic and adherent *Staphylococcus aureus ACS Appl. Mater. Interfaces* **9** 25691–9

[23] Croes M *et al* 2018 Antibacterial and immunogenic behavior of silver coatings on additively manufactured porous titanium *Acta Biomater.* **81** 315–27

[24] Van Hengel I A *et al* 2017 Selective laser melting porous metallic implants with immobilized silver nanoparticles kill and prevent biofilm formation by methicillin-resistant *Staphylococcus aureus Biomaterials* **140** 1–15

[25] Croes M *et al* 2017 Local induction of inflammation affects bone formation *Eur. Cells Mater.* **33** 211–26

[26] Brown B N, Ratner B D, Goodman S B, Amar S and Badylak S F 2012 Macrophage polarization: an opportunity for improved outcomes in biomaterials and regenerative medicine *Biomaterials* **33** 3792–802

[27] Franz S, Rammelt S, Scharnweber D and Simon J C 2011 Immune responses to implants–a review of the implications for the design of immunomodulatory biomaterials *Biomaterials* **32** 6692–709

[28] Sridharan R, Cameron A R, Kelly D J, Kearney C J and O'Brien F J 2015 Biomaterial based modulation of macrophage polarization: a review and suggested design principles *Mater. Today* **18** 313–25

[29] Bai L *et al* 2018 A multifaceted coating on titanium dictates osteoimmunomodulation and osteo/angio-genesis towards ameliorative osseointegration *Biomaterials* **162** 154–69

[30] Chen Z *et al* 2017 Tuning chemistry and topography of nanoengineered surfaces to manipulate immune response for bone regeneration applications *ACS Nano* **11** 4494–506

[31] Chen Z *et al* 2017 Nanotopography-based strategy for the precise manipulation of osteoimmunomodulation in bone regeneration *Nanoscale* **9** 18129–52

[32] Chen Z *et al* 2018 Immunomodulatory effects of mesoporous silica nanoparticles on osteogenesis: from nanoimmunotoxicity to nanoimmunotherapy *Appl. Mater. Today* **10** 184–93

[33] Chen Z *et al* 2016 Osteoimmunomodulation for the development of advanced bone biomaterials *Mater. Today* **19** 304–21

[34] Chen Z, Yuen J, Crawford R, Chang J, Wu C and Xiao Y 2015 The effect of osteoimmunomodulation on the osteogenic effects of cobalt incorporated β-tricalcium phosphate *Biomaterials* **61** 126–38

[35] Li B, Gao P, Zhang H, Guo Z, Zheng Y and Han Y 2018 Osteoimmunomodulation, osseointegration, and *in vivo* mechanical integrity of pure Mg coated with HA nanorod/pore-sealed MgO bilayer *Biomater. Sci.* **6** 3202–18

[36] Sadowska J M, Wei F, Guo J, Guillem-Marti J, Ginebra M-P and Xiao Y 2018 Effect of nano-structural properties of biomimetic hydroxyapatite on osteoimmunomodulation *Biomaterials* **181** 318–32

[37] Lü W, Wang N, Gao P, Li C, Zhao H and Zhang Z 2015 Effects of anodic titanium dioxide nanotubes of different diameters on macrophage secretion and expression of cytokines and chemokines *Cell Proliferation* **48** 95–104

[38] Ma Q-L *et al* 2014 Improved implant osseointegration of a nanostructured titanium surface via mediation of macrophage polarization *Biomaterials* **35** 9853–67

[39] Tan J *et al* 2016 Nano-topographic titanium modulates macrophage response *in vitro* and in an implant-associated rat infection model *RSC Adv.* **6** 111919–27

[40] Zhang Z, Xie Y, Pan H, Huang L and Zheng X 2018 Influence of patterned titanium coatings on polarization of macrophage and osteogenic differentiation of bone marrow stem cells *J. Biomater. Appl.* **32** 977–86

[41] Alfarsi M A, Hamlet S M and Ivanovski S 2014 Titanium surface hydrophilicity modulates the human macrophage inflammatory cytokine response *J. Biomed. Mater. Res.* A **102** 60–7

[42] Barth K A, Waterfield J D and Brunette D M 2013 The effect of surface roughness on RAW 264.7 macrophage phenotype *J. Biomed. Mater. Res.* A **101** 2679–88

[43] Jain N and Vogel V 2018 Spatial confinement downsizes the inflammatory response of macrophages *Nat. Mater.* **17** 1134

[44] Wang G, Wan Y and Liu Z 2018 Incorporation of antibacterial ions on the micro/nanostructured surface and its effects on the corrosion behavior of titanium *Mater. Lett.* **216** 303–5

[45] Karageorgiou V and Kaplan D 2005 Porosity of 3D biomaterial scaffolds and osteogenesis *Biomaterials* **26** 5474–91

[46] Taniguchi N *et al* 2016 Effect of pore size on bone ingrowth into porous titanium implants fabricated by additive manufacturing: an *in vivo* experiment *Mater. Sci. Eng.* C **59** 690–701

[47] Necula B S, Fratila-Apachitei L E, Zaat S A, Apachitei I and Duszczyk J 2009 *In vitro* antibacterial activity of porous TiO$_2$–Ag composite layers against methicillin-resistant *Staphylococcus aureus Acta Biomater.* **5** 3573–80

[48] Fahy N *et al* 2014 Human osteoarthritic synovium impacts chondrogenic differentiation of mesenchymal stem cells via macrophage polarisation state *Osteoarthritis Cartilage* **22** 1167–75

[49] Grotenhuis N, Bayon Y, Lange J, Van Osch G and Bastiaansen-Jenniskens Y 2013 A culture model to analyze the acute biomaterial-dependent reaction of human primary macrophages *Biochem. Biophys. Res. Commun.* **433** 115–20

[50] Knuth C A *et al* 2018 Isolating pediatric mesenchymal stem cells with enhanced expansion and differentiation capabilities *Tissue Eng.* C **24** 313–21

[51] Spiller K L *et al* 2016 Differential gene expression in human, murine, and cell line-derived macrophages upon polarization *Exp. Cell. Res.* **347** 1–13

[52] Kaneshiro S *et al* 2014 IL-6 negatively regulates osteoblast differentiation through the SHP2/MEK2 and SHP2/Akt2 pathways *in vitro J. Bone Mineral Metab.* **32** 378–92

[53] Gallucci R M *et al* 2000 Impaired cutaneous wound healing in interleukin-6–deficient and immunosuppressed mice *The FASEB J.* **14** 2525–31

[54] Jilka R L *et al* 1992 Increased osteoclast development after estrogen loss: mediation by interleukin-6 *Science* **257** 88–91

[55] Nie B, Ao H, Zhou J, Tang T and Yue B 2016 Biofunctionalization of titanium with bacitracin immobilization shows potential for anti-bacteria, osteogenesis and reduction of macrophage inflammation *Colloids Surf.* B **145** 728–39

[56] Omar O M *et al* 2011 The correlation between gene expression of proinflammatory markers and bone formation during osseointegration with titanium implants *Biomaterials* **32** 374–86

[57] Wang Y-W, Xu D-P, Liu Y, Zhang R and Lu L 2015 The effect of tumor necrosis factor-α at different concentrations on osteogenetic differentiation of bone marrow mesenchymal stem cells *J. Craniofacial Surg.* **26** 2081–5

[58] Frost A, Jonsson K B, Nilsson O and Ljunggren Ö 1997 Inflammatory cytokines regulate proliferation of cultured human osteoblasts *Acta Orthopaedica Scand.* **68** 91–6

[59] Gu Q, Yang H and Shi Q 2017 Macrophages and bone inflammation *J. Orthopaedic Transl.* **10** 86–93

[60] Fenton M J, Buras J A and Donnelly R P 1992 IL-4 reciprocally regulates IL-1 and IL-1 receptor antagonist expression in human monocytes *J Immunol* **149** 1283–8

[61] Moura C C G, Soares P B F, Souza M A D and Zanetta-Barbosa D 2011 Effect of titanium surface on secretion of IL1β and TGFβ1 by mononuclear cells *Braz. Oral Res.* **25** 500–5

[62] Champagne C, Takebe J, Offenbacher S and Cooper L 2002 Macrophage cell lines produce osteoinductive signals that include bone morphogenetic protein-2 *Bone* **30** 26–31

[63] Rees P A, Greaves N S, Baguneid M and Bayat A 2015 Chemokines in wound healing and as potential therapeutic targets for reducing cutaneous scarring *Adv. Wound Care* **4** 687–703

[64] Huang Q *et al* 2018 The Cu-containing TiO$_2$ coatings with modulatory effects on macrophage polarization and bactericidal capacity prepared by micro-arc oxidation on titanium substrates *Colloids Surf.* B **170** 242–50

[65] Zhang X-F, Shen W and Gurunathan S 2016 Silver nanoparticle-mediated cellular responses in various cell lines: an *in vitro* model *Int. J. Mol. Sci.* **17** 1603

[66] Singh R P and Ramarao P 2012 Cellular uptake, intracellular trafficking and cytotoxicity of silver nanoparticles *Toxicol. Lett.* **213** 249–59

[67] Vasconcelos D P, Águas A P, Barbosa M A, Pelegrín P and Barbosa J N 2019 The inflammasome in host response to biomaterials: bridging inflammation and tissue regeneration *Acta Biomater.* **83** 1–12

[68] Yang E-J, Kim S, Kim J S and Choi I-H 2012 Inflammasome formation and IL-1β release by human blood monocytes in response to silver nanoparticles *Biomaterials* **33** 6858–67